Experimental study of a 3D-printed wick condenser for enhanced condensation heat transfer

Jay Saple¹¹, Behzad Ahmadi¹¹, Mohammad Reza Shaeri², Sajjad Bigham^{1*}

¹Department of Mechanical and Aerospace Engineering, North Carolina State University, Raleigh, NC, 27695-7910, USA

²Advanced Cooling Technologies, Inc., Pennsylvania, USA

¹ Same contribution

* corresponding author: sbigham@ncsu.edu

Existing methods for improving condensation heat transfer face challenges with low surface tension liquids that exhibit strong wetting properties. These liquids tend to condense as thin films, leading to suboptimal thermal performance. This study investigates the effectiveness of a novel 3D-printed wick condenser in enhancing the condensation heat transfer rate of low surface tension fluids. An experimental test facility is developed to compare the heat dissipation performance of the 3D-printed wick condenser with a plain surface. The wick condenser, 3D-printed using GRCop-42 with an effective thermal conductivity of 344 W/m-K at room temperature, demonstrates remarkable heat flux capabilities. For example, at a subcooling of 10.5°C, the new 3Dprinted wick condenser achieves a heat flux of about 61 kW/m² with the low-surface-tension fluid HFE-7100, representing a 4-fold improvement compared to a plain copper surface. The insights gained from this study open up exciting possibilities for the development of next-generation condensation surface technologies that offer unprecedented heat transfer rates, especially for liquids with complete wetting behavior.

Keywords: Wick condenser; Low surface tension fluids; Additive manufacturing; Experimental evaluation; Condensation heat transfer rate.

I. INTRODUCTION

In recent decades, extensive research has been dedicated to enhancing the condensation heat transfer process, a pursuit with the potential to elevate energy efficiency and alleviate capital costs. This improved condensation rate holds substantial relevance across diverse industrial applications, including but not limited to desalination [1]–[3], air conditioning and refrigeration [4]–[6], distillation, water harvesting [7], [8], humidity sensors [9], electronic cooling as well as power plant thermal management [10]–[13].

Traditionally employed metallic condenser surfaces often promote filmwise condensation, leading to relatively inefficient heat transfer performance. This is primarily attributed to the development of a thick liquid layer, introducing significant thermal resistance between the cold condenser surface and the condensing vapor. Numerous experimental and numerical studies have been conducted to enhance condensation heat transfer rates by exploring novel condenser surfaces that leverage a dropwise condensation mechanism. In the dropwise

condensation process, droplets of varying sizes are formed, which, upon reaching a critical radius, detach from the surface. This shedding action exposes the cold condenser surface to vapor for further condensation, improving overall efficiency. To achieve the dropwise condensation mode of heat transfer, various methods, such as micro and nanoscale structures promoting superhydrophobic surfaces, surface coating, and slippery liquid-infused porous surfaces (SLIPS), have been employed.

Nano-textured surfaces, including copper oxide layers [14], copper nanowires [15], and micro-nano hierarchical structures [16], boost condensation heat transfer by fostering dropwise condensation through the creation of superhydrophobic surfaces showing low contact angle hysteresis, increasing nucleation sites, and providing a larger surface area for efficient heat transfer. Milkjkovic et al. [14] employed a sharp, knife-like CuO layer to improve condensation by promoting the jumping droplets. In this process, coalescing droplets are expelled from a superhydrophobic nanostructured surface, facilitated by the release of excess surface energy. While this mechanism allows for efficient heat dissipation at low sub-cooled temperatures, issues such as flooding can arise at higher sub-cooled temperatures, leading to a decline in performance [14][15]. Another approach demonstrated by Varanasi et al. [17] showed that the local wettability of a surface can be manipulated by patterning with a mix of hydrophobic and hydrophilic regions. This results in spatial control in the heterogeneous nucleation instead of the random nucleation behavior of superhydrophobic surfaces, resulting in enhanced condensation heat transfer.

Coatings offer an alternative solution for achieving dropwise condensation, mitigating challenges related to nanostructure fabrication and concerns associated with flooding regimes. These coatings can be applied to plain surfaces or in conjunction with microstructures. Wang et al. [18] employed a double lithography process to coat micropillars with a hydrophobic fluorosilane, resulting in a hierarchical hydrophobic surface. Experimental tests demonstrated that consistent performance could be maintained over a significantly large sub-cooling range of approximately 25°C. In a study by Thomas et al. [19], various

hydrophobic coatings, including perfluoro-octyl-triethoxy-silane and perfluoro-octanoic-acid, were compared with a commercially available Glaco solution on micro-nano hierarchical structures. Despite Glaco exhibiting a jumping droplet mechanism, the silane and octanoic acid coatings outperformed the Glaco solution. Additionally, Cha et al. [20] indicated that a hydrophobic surface is not mandatory for dropwise condensation; rather, a surface with low contact angle hysteresis is crucial. Their findings showed that PEGylated hydrophilic surfaces, despite being hydrophilic, exhibited higher nucleation compared to fluorinated hydrophobic surfaces. This suggests a potential avenue for future research in surfaces that are both hydrophilic and exhibit high mobility.

A different approach inspired by the Nepenthes pitcher plant was adopted by Wong et al. [21]. They introduced a lubricant liquid trapped between nanostructures, creating an omniphobic surface that allows condensed fluid to effortlessly roll off. Using this method, Rykaczewski et al. [22] demonstrated dropwise condensation for low-surface tension fluids. Since an air gap is not necessary to maintain a slippery surface, this approach gives a pressure-stable slippery surface [21]. However, Adera et al. [23] highlighted some practical limitations to the lubricantbased approach. As the condensed liquid droplets are released from the surface, sometimes a small part of the droplet remains on the surface, known as satellite droplets. Moreover, there are very few lubricating liquids that have very low miscibility with low surface tension fluids. Furthermore, cloaking occurs when the spreading coefficient of the oil on the liquid is greater than zero, leading to the encapsulation of the liquid by the lubricant. This process inhibits droplet growth and increases thermal resistance [24].

While the approaches mentioned above effectively enhance the condensation heat transfer rate of high surface tension fluids, they often fall short or underperform when applied to low surface tension fluids such as refrigerants, fluorinated dielectrics, and hydrocarbons due to their highly wetting behavior. To tackle this challenge, this study proposes a novel 3D-printed wick condenser. The innovative wick condenser comprises alternating wick structures and plain surfaces. The newly designed wick condenser surface, 3D-printed with copper, is tested with HFE-7100 working fluid under stationary condensation conditions. In the subsequent sections, we first delve into the concept of the wick condenser. Then, the experimental setup and the 3D printing of the wick condenser are discussed. Finally, the experimentally measured condensation heat flux of the 3D-printed wick condenser with that of a plain copper surface are compared.

II. CONCEPT: WICK CONDENSER

In existing state-of-the-art enhanced condensation heat transfer surfaces, the same surface serves both the droplet formation/growth process and the removal of condensed liquid. This sets up a competition between the condensing surface and shedding paths. The proposed wick condenser introduces a wick condensation surface to separate the condensing surface from condensate shedding paths. Illustrated in Fig. 1a, the wick condenser consists of alternating wick structures and plain surfaces. The active condensing surfaces include the side and

top surfaces of the wick structure, as well as the plain channel area.

In a traditional condensing surface, increasing the condensation rate typically results in a thicker condensate layer, introducing significant thermal resistance. In contrast, the proposed wick condenser leverages the capillary effect to wick the condensate from the vapor-exposed surfaces into the wick structure, as depicted in Fig. 1b. Despite the low surface tension of HFE-7100, the described wicking action occurs on a short length scale below the capillary length scale. Upon condensate wicking, the collected condensate is drained through the inner part of the wick structure under the influence of gravity, as shown in Fig. 1c. Consequently, the active condensing surfaces (i.e., plain channel area and side/top wick surface) are effectively decoupled from the liquid shedding pathway (i.e., the inner part of the wick structure). This approach is a passive method with no moving parts for condensate removal. Additionally, the condenser's performance is less susceptible to degradation over time, as no coating layer is employed [25].

III. EXPERIMENTAL SECTION

In this section, first, the fabrication procedure of the wick condenser utilizing the additive manufacturing method is explained. Then, the experimental test facility developed for evaluating the performance of the wick condenser under stationary condensation conditions is discussed in detail. Finally, data reduction and uncertainty analysis associated with the experimental results are presented.

A. 3D printing of wick condenser

Advanced additive manufacturing techniques enable the realization of intricate heat transfer topologies [28]–[31]. The proposed wick condenser was 3D-printed using the selective laser melting (SLM) method with the EOS M290 3D printer. The EOS M290 printer utilizes a 400 W power laser with a focus diameter of 100 microns. To take advantage of its high thermal

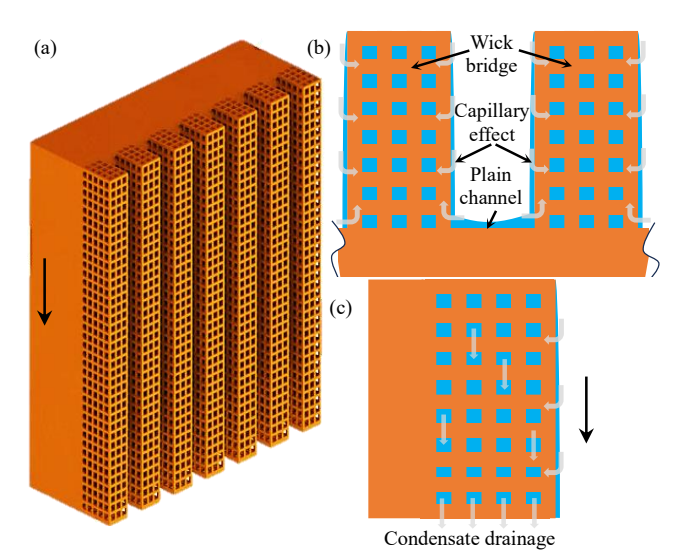


Fig. 1. (a) A 3D schematic of the wick condenser with alternative plain channels and wick structures, (b) condensate is wicked into the inner section of the wick structures (top-view of condenser), and (c) condensate drains under the influence of gravity (side-view of condenser).

conductivity of about 344 W/m-K at room temperature, copper alloy GRCop-42 (94% copper, 4% chromium, and 2% niobium) developed by NASA was used for printing of wick condenser.

Fig. 2 shows images and a schematic view of the 3D-printed wick condenser, providing insight into its geometrical dimensions. The base of the 3D-printed condenser has a cross-sectional area of $20.3 \times 20.3 \text{ mm}^2$ with a height of 6.35 mm. The wick structures are 3.3 mm in height and 0.65 mm in width. The pore size and wall thickness of the wick structure are $50 \text{ and } 300 \text{ }\mu\text{m}$, espec el . Add on ll , he w d h of he pl n ch nnel measures 1.35 mm. The 3D-printed wick condenser is composed of 11 wick structures and 10 plain channels. It should be noted h he w ll h ckness of he w ck s uc u e (.e., $300 \text{ }\mu\text{m}$) aligns with the constraints of the available copper 3D printer, as printing thinner copper walls poses challenges.

The 3D-printed wick condenser was submerged in Isopropyl Alcohol (IPA) in an ultrasonic cleaner bath for powder removal. After one hour of ultrasonic cleaning, a high-pressure compressed air stream was employed to remove any trapped powder inside the wick structure. This process was repeated several times to ensure all particles were extracted from the wick structure. The particle size distribution of the GRCop-42 powder is shown in Fig. 3. As shown, 100% of the particles can pass h ou h po e s ze of 50 μm . Add on ll , he w ck condense s were examined under a microscope to explore the possibility of any trapped powder. As shown in Fig. 2b, the ultrasonic cleaning procedure was able to remove all powders from the wick structure.

B. Experimental test setup

Fig. 4 shows a schematic view of the test facility designed for performance evaluation of the 3D-printed wick condenser exposed to saturated stationary vapor. The test apparatus consists of three main parts: the 3D-printed wick condenser, a 1D heat transfer column, and a water-cooled milli-channel heat exchanger (HX). The condenser surface was soldered to the 1D heat transfer column to minimize contact thermal resistance between the condenser surface and the 1D heat transfer column. Both the 1D heat transfer column and milli-channel HX were

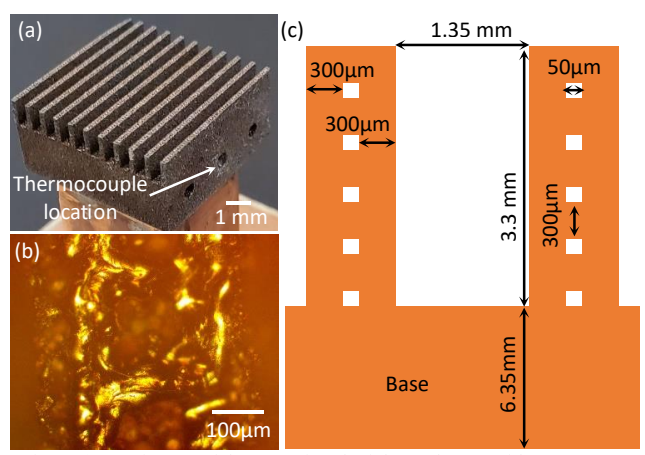


Fig. 2. (a) An image of the 3D-printed wick condenser with GRCop-42, (b) a microscopic image of the wick structure, and (c) a schematic view of the printed wick condenser including geometrical dimensions (not scaled).

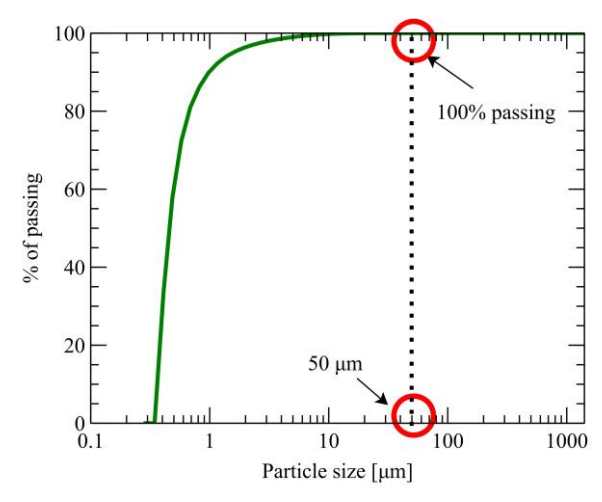


Fig. 3. Particle size distribution for the GRCop 42 powder employed.

made of copper to minimize thermal resistance between the 1D column and the cooling water.

The dimensions of the 1D column include a cross-sectional area of 15.7 x 15.7 mm² and a length of 2.5 cm. Utilizing a chiller, a cooling water stream with a temperature below the saturation temperature of the working fluid was pumped through the milli-channel HX. The test apparatus assembly was embedded in a PTFE insulation to minimize heat gain. Using Fou e 's l w of he conduc on, he expe men l condens on heat flux was measured utilizing the temperature values of the 1D column in three places (i.e., T₂, T₃, and T₄). The temperature of the liquid-solid interface (T_s) was extrapolated using thermocouples embedded in the condenser base (i.e., T₁) and experimentally measured condensation heat flux.

The test apparatus was inserted into a vacuum chamber as shown in Fig. 4a. The vacuum chamber consists of a thermocouple feedthrough, a viewport, a pressure transducer, and multiple valves. Initially, the vacuum chamber was partially filled with the working fluid. In the current study, Novec 7100 was chosen as an example working fluid with a very low surface tension. The saturation pressure of the condensation chamber was initially established by an external heater. Then, the temperature of the condenser surface was reduced to a temperature lower than the saturation temperature by passing a cold water stream through the cooling milli-channel HX utilizing a tube feedthrough connection. This allows the establishment of different sub-cooled temperatures. A vacuum pressure transducer (Setra P/N 730G) was employed to measure pressure inside the chamber with an accuracy of $\pm 0.1\%$ reading. Also, temperatures at different locations were measured utilizing various T-type thermocouples (Omega TMTSS-062U) with an accuracy of ±0.3°C. A data acquisition system (KEYSIGTH 34972A) was utilized to record the experimental data at a frequency of 1 Hz. It is worth mentioning that the accuracy of the condensation test setup and test procedure was initially examined for a plain copper surface and compared against Nusselt's theory of vertical falling film condensation.

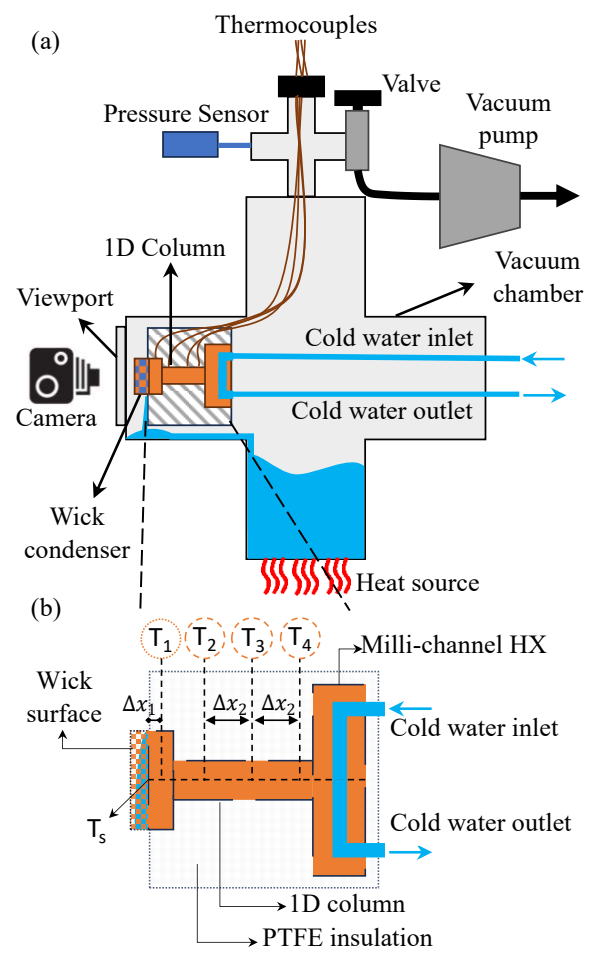


Fig. 4. (a) A schematic of the stationary condensation test facility, and (b) a schematic of the 1D heat transfer column connected to the water-cooler heat exchanger.

C. Data reduction and uncertainty analysis

The experimentally measured heat flux $(q_{exp}^{"})$ and the condenser surface temperature at the solid-liquid interface (T_s) are c lcul ed us n Fou e 's l w of he conduc on as follows:

$$q_{exp}^{"} = k_s(\Delta T_{1D})(A_{1D}/A_{cond})/(2\Delta x_2)$$
 (1)

$$T_{\rm S} = T_1 + \Delta x_1 q_{\rm exp}^{"}/k_{\rm S} \tag{2}$$

where k_s , A_{1D} , A_{cond} , and ΔT_{1D} are the copper thermal conductivity, the cross-sectional area of the 1D heat transfer column, the condenser surface area, and the temperature difference across the 1D heat transfer column. The experimental results obtained from the plain copper condensing surface are validated against Nusselt's theory of film condensation. The analytical Nusselt heat flux of condensation $(q_{Nu}^{"})$ for a vertical plain surface can be written as follows:

$$q_{Nu}^{"} = 0.943 \left[\frac{\rho_l(\rho_l - \rho_v) g h_{fg}^{\prime} k_l^3 (T_{sat} - T_s)^3}{\mu_l L} \right]^{1/4}$$
 (3)

where ρ_l , ρ_v , h'_{fg} , k_l , and μ_l are liquid density, vapor density, heat of vaporization, thermal conductivity, and dynamic

viscosity of working fluid. Also, the heat transfer coefficient (HTC) is calculated as follows:

$$HTC = \frac{q_{exp}^{"}}{\Delta T_{sub-cooled}} \tag{4}$$

where $\Delta T_{sub-cooled} = (T_{saturation@p} - T_s)$ is the sub-cooled temperature. The uncertainty associated with the experimentally measured heat flux, the condenser surface temperature at the solid-liquid interface, and the HTC can be calculated as follows:

$$\frac{\delta q_{exp}^{"}}{q_{exp}^{"}} = \sqrt{\left(\frac{\delta \Delta T_{1D}}{\Delta T_{1D}}\right)^2 + \left(\frac{\delta \Delta x_2}{\Delta x_2}\right)^2 + \left(\frac{\delta A_{1D}}{A_{1D}}\right)^2 + \left(\frac{\delta A_{cond}}{A_{cond}}\right)^2}$$
(5)

$$\frac{\delta T_s}{T_s} = \sqrt{\left(\frac{\delta T_1}{T_1}\right)^2 + \left(\frac{\delta \Delta x_1}{\Delta x_1}\right)^2 + \left(\frac{\delta q_{exp}^{"}}{q_{exp}^{"}}\right)^2} \tag{6}$$

$$\frac{\delta HTC}{HTC} = \sqrt{\left(\frac{\delta \Delta T_{sub-cooled}}{\Delta T_{sub-cooled}}\right)^2 + \left(\frac{\delta q_{exp}^"}{q_{exp}^"}\right)^2}$$
(7)

IV. RESULTS AND DISCUSSION

Fig. 5 shows the experimentally measured average condensation heat flux of the 3D-printed copper wick and plain condensers plotted against sub-cooled temperatures. The experiments were conducted using HFE Novec-7100 as a representative low-surface tension fluid. In both the 3D-printed wick and plain condensation surfaces, the condensation heat flux exhibits an increase with sub-cooled temperature, attributed to the augmented driving force for the condensation process. The figure also includes a comparison of the experimental results with Nusselt's theory of vertical falling film condensation. Notably, the experimentally measured condensation heat flux data for the plain condenser surface reasonably aligns with Nusselt's theory of film condensation.

The results clearly indicate that the 3D-printed copper wick condenser significantly improves the condensation heat transfer

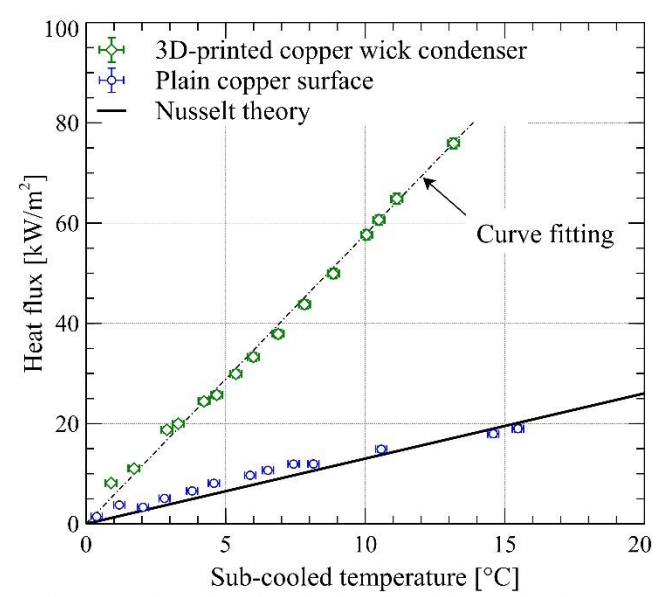


Fig. 5. Experimental condensation heat flux of the 3D-printed copper wick and plain condensers versus sub-cooled temperature.

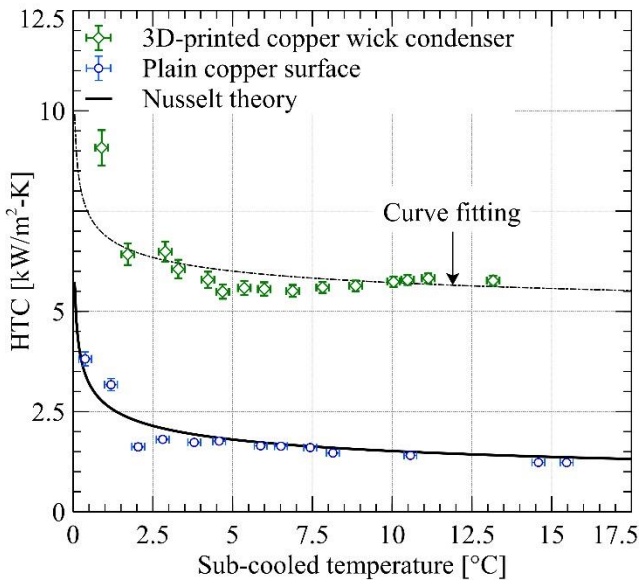


Fig. 6. Variation of heat transfer coefficient of the 3D-printed copper wick and plain condenser surfaces as a function of sub-cooled temperature.

rate compared to the plain copper surface. This is attributed to the topology of the wick condenser that decouples the condensation surface from the shedding surface. For instance, at a sub-cooled temperature of 10.5° C, the condensation heat flux increases from about 15 kW/m^2 on the plain copper surface to about 61 kW/m^2 on the 3D-printed copper wick condenser, leading to a 306% improvement in the condensation heat flux.

Fig. 6 shows the HTC versus the sub-cooled temperature for the 3D-printed copper wick and plain condensers and Nusselt's theory of film condensation. The Nusselt theory of film condensation suggests a high dependence of the HTC on sub-cooled temperature at low sub-cooled temperatures, whereas the dependency becomes negligible at a higher sub-cooled temperature. The same trend can be seen in the experimental results of both 3D-printed wick and plain condenser surfaces. More importantly, a stark increase in the heat transfer capacity can be observed from the plain surface to the wick condenser. For example, the HTC increases from 1.47 kW/m²-K on the plain condenser surface to 5.8 kW/m²-K on the 3D-printed copper wick condenser at a sub-cooled temperature of 10.5°C, resulting in a 310% improvement.

V. CONCLUSION

In summary, this study introduces a novel 3D-printed copper wick condenser to enhance the condensation heat transfer process of low surface tension liquids. The 3D-printed wick condenser consists of several alternative wick structures and plain surfaces. The wick condenser was 3D-printed utilizing the SLM method with copper alloy GRCop-42. The condensation performance of the 3D-printed wick condenser was tested using HFE Novec-7100 as a working fluid. The experimental results indicated the 3D-printed wick condenser provides almost 4 times higher condensation heat flux compared with its plain surface counterpart at a sub-cooled temperature of 10.5°C. The results achieved here provide a pathway to develop new

condensation surfaces, offering superior performance compared with conventional condensation surfaces.

DECLARATION OF COMPETING INTEREST

The authors declare that they have no known competing financial interests or personal relationships that could have appeared to influence the work reported in this paper.

REFERENCES

- [1] C. Du, D. H n, nd C. Hu n, "Enh nced po condens on b he m l redistribution on the evaporation surface in heat-loc l zed sol des l n on," *Appl Therm Eng*, vol. 215, Oct. 2022, doi: 10.1016/j.applthermaleng.2022.118941.
- [2] A. K. Thakur, R. Sathyamurthy, R. Velraj, R. Saidur, and J. Y. Hwang, "Au men ed pe fo m nce of sol des l n on un b u l z on of n no-silicon coated glass cover for promoting drop-w se condens on," *Desalination*, vol. 515, Nov. 2021, doi: 10.1016/j.desal.2021.115191.
- [3] N. Luk c, L. L. D ezel, A. P. F öb , nd A. Le pe z, "Econom c 1 spec s of the improvement of a mechanical vapour compression desalination plant by d opw se condens on," *Desalination*, vol. 264, no. 1–2, pp. 173–178, Dec. 2010, doi: 10.1016/j.desal.2010.07.023.
- [4] A. Cavallini *et al.*, "Condens on ns de nd ou s de smoo h nd enh nced tubes e ew of ecen ese ch," *International Journal of Refrigeration*, vol. 26, no. 4. Elsevier Ltd, pp. 373–392, 2003. doi: 10.1016/S0140-7007(02)00150-0.
- [5] A. Cavallini, G. Censi, D. Del Col, L. Doretti, G. A. Longo, and L. Rosse o, "Expe men 1 n es on on condens on he nsfe nd pressure drop of new HFC refrigerants (R134a, R125, R32, R410A, R236ea) in ho zon 1 smoo h ube," 2001. [Online]. Available: www.elsevier.com/locate/ijrefrig
- [6] A. M., K. Non k., and M. T. n. uch, "Condens on he nsfe and flow pattern inside a herringbone-type micro-f n. ube," *International Journal of Refrigeration*, vol. 23, no. 2, pp. 141–152, Mar. 2000, doi: 10.1016/S0140-7007(99)00037-7.
- [7] J. Ju, H. B , Y. Zhen , T. Zh o, R. F n , nd L. J n , "A mul -structural and multi-func on l n e $\,$ ed fo collec on s s em n c c us," Nat Commun, vol. 3, 2012, doi: 10.1038/ncomms2253.
- [8] S. C. Th cke , C. Ne o, nd A. T. H s, "B om me c su f ce co n s fo mosphe c w e c p u e p ep ed b dewe n of pol me f lms," Advanced Materials, vol. 23, no. 32, pp. 3718–3722, Aug. 2011, doi: 10.1002/adma.201100290.
- [9] J. T. W. Yeow and J. P. M. She, "C bon n no ube-enhanced capillary condens on fo c p c e hum d senso," *Nanotechnology*, vol. 17, no. 21, pp. 5441–5448, Nov. 2006, doi: 10.1088/0957-4484/17/21/026.
- [10] R. N. Le ch, F. S e ens, S. C. L n fo d, nd J. T. D ck nson, "D opw se Condensation: Experiments and Simulations of Nucleation and Growth of W e D ops n Cool n S s em," *Langmuir*, vol. 22, no. 21, pp. 8864–8872, Oct. 2006, doi: 10.1021/la061901+.
- [11] S. D n el, M. K. Ch udhu, nd J. C. Chen, "F s D op Mo emen s Resul n f om he Ph se Ch n e on G d en Su f ce," *Science* (1979), vol. 291, no. 5504, pp. 633–636, 2001, doi: 10.1126/science.291.5504.633.
- [12] K. Rykaczewski, J. H. J. Scott, S. Rajauria, J. Chinn, A. M. Chinn, and W. Jones, "Th ee d mens on 1 spec s of d ople co lescence du n d opw se condens on on supe h d ophob c su f ces," *Soft Matter*, vol. 7, no. 19, pp. 8749–8752, Oct. 2011, doi: 10.1039/c1sm06219k.
- [13] X. Chen *et al.*, "N no ssed m c op m d 1 ch ec u es fo con nuous d opw se condens on," *Adv Funct Mater*, vol. 21, no. 24, pp. 4617–4623, Dec. 2011, doi: 10.1002/adfm.201101302.
- [14] N. Miljkovic *et al.*, "Jump n -droplet-enhanced condensation on scalable supe h d ophob c n nos uc u ed su f ces," *Nano Lett*, vol. 13, no. 1, pp. 179–187, Jan. 2013, doi: 10.1021/nl303835d.
- [15] R. Wen *et al.*, "H d ophob c coppe n now es fo enh nc n condens on he nsfe," *Nano Energy*, vol. 33, pp. 177–183, Mar. 2017, doi: 10.1016/j.nanoen.2017.01.018.
- [16] X. W n , B. Xu, Q. L u, Y. Y n , nd Z. Chen, "Enh ncemen of po condensation heat transfer on the micro- and nano-structured superhydrophobic

- su f ces," Int J Heat Mass Transf, vol. 177, Oct. 2021, doi: 10.1016/j.ijheatmasstransfer.2021.121526.
- [17] K. K. V n s , M. Hsu, N. Bh e, W. Y n , nd T. Den , "Sp 1 con ol n he he e o eneous nucle on of w e ," *Appl Phys Lett*, vol. 95, no. 9, 2009, doi: 10.1063/1.3200951.
- [18] X. W n , B. Xu, Q. L u, Y. Y n , nd Z. Chen, "Enh ncemen of po condensation heat transfer on the micro- and nano-structured superhydrophobic su f ces," *Int J Heat Mass Transf*, vol. 177, Oct. 2021, doi: 10.1016/j.ijheatmasstransfer.2021.121526.
- [19] T. M. Thom s nd P. S nh M h p , "Condens on of Hum d A on Superhydrophobic Surfaces: Effect of Nanocoatings on a Hierarchical In e f ce," *Langmuir*, vol. 37, no. 44, pp. 12767–12780, Nov. 2021, doi: 10.1021/acs.langmuir.1c01012.
- [20] H. Cha *et al.*, "D opw se condens on on sold h d oph l c su f ces," 2020. [Online]. Available: https://www.science.org
- [21] T. S. Wong *et al.*, "B o nsp ed self-repairing slippery surfaces with pressure-s ble omn phob c ," *Nature*, vol. 477, no. 7365, pp. 443–447, Sep. 2011, doi: 10.1038/nature10447.
- [22] K. Rykaczewski *et al.*, "D opw se condens on of low su f ce ens on flu ds on omn phob c su f ces," *Sci Rep*, vol. 4, Mar. 2014, doi: 10.1038/srep04158.
- [23] S. Adera, J. Alvarenga, A. V. Shneidman, C. T. Zhang, A. Davitt, and J. A zenbe , "Deple on of Lub c n f om N nos uc u ed O l-Infused Surfaces b Pend n Condens e D ople s," *ACS Nano*, vol. 14, no. 7, pp. 8024–8035, Jul. 2020, doi: 10.1021/acsnano.9b10184.
- [24] S. Se, X. Yn, G. B, c, L. W. Bolon, nd N. Mljko, c, "Lub cn-Infused Surfaces for Low-Surface-Tens on Flu ds: P om se, e sus Re 1," ACS Appl Mater Interfaces, vol. 9, no. 41, pp. 36400–36408, Oct. 2017, doi: 10.1021/acsami.7b10756.
- [25] Y.-T. Chen nd D. E. Rod k, "Is he lo us le f supe h d ophob c?," *Appl Phys Lett*, vol. 86, no. 14, p. 144101, Mar. 2005, doi: 10.1063/1.1895487.
- [26] G. V. Du m, "CAPILLARY-ASSISTED ENHANCED CONDENSATION HEAT TRANSFER FOR LOW SURFACE TENSION LIQUIDS," M ch n Technolo c l Un e s , Hou h on, M ch n, 2018. doi: 10.37099/mtu.dc.etdr/574.
- [27] P. Gradl *et al.*, "Ad nœmen of ex eme en onmen dd el m n uf c u ed llo s fo nex ene on sp ce p opuls on ppl c ons," *Acta Astronaut*, vol. 211, pp. 483–497, Oct. 2023, doi: 10.1016/j.actaastro.2023.06.035.
- [28] B. Ahm d nd S. B h m, "Pe fo m n ce E lu on of h -k Lung-inspired 3D-p n ed Pol me He Exch n e s," *Appl Therm Eng*, vol. 204, p. 117993, 2022, doi: https://doi.org/10.1016/j.applthermaleng.2021.117993.
- [29] B. Ahm d, J. Ces no, K. N w z, N. N nos, nd S. B h m, "A h h-performance lung-inspired ceramic 3D-printed heat exchanger for high-temperature energy-eff c en s s ems," *Appl Therm Eng*, vol. 219, p. 119378, 2023, doi: https://doi.org/10.1016/j.applthermaleng.2022.119378.
- [30] U. Pu u, M. Ahm d, B. Ahm d, nd S. B h m, "A no el lun-inspired 3D-printed desiccant-coated heat exchanger for high-performance humidity m n emen n bu ld n s," *Energy Convers Manag*, vol. 252, p. 115074, 2022, doi: https://doi.org/10.1016/j.enconman.2021.115074.
- [31] B. Ahmadi, J. Cesarano, K. Nawaz, N. Ninos, and S. Bigham, "CERAMIC 3D-PRINTED HEAT EXCHANGERS FOR HIGH-TEMPERATURE HEAT RECOVERY," n *Proceedings of the Thermal and Fluids Engineering Summer Conference*, Begell House Inc., 2022, pp. 1285–1288. doi: 10.1615/tfec2022.tes.040984.